Neoplasma 2024; 71(3): 279–288

doi:10.4149/neo_2024_240312N111

Circular RNA IARS modulates the progression and ferroptosis of osteosarcoma via sponging miR-188-5p from RAB14

Yafei LI[1,#], Yan ZHANG[1,#], Xiaohong LU[1], Ruie LI[1], Jiayu PENG[1], Yangbo XU[2,*]

[1]Department of Oncology, Luzhou People's Hospital, Luzhou, Sichuan, China; [2]Department of Bone and Joint Surgery, Affiliated Hospital of Southwest Medical University, Luzhou, Sichuan, China

**Correspondence: yangboxusmu@21cn.com*
#Contributed equally to this work.

Received March 12, 2024 / Accepted June 17, 2024

Osteosarcoma (OS) is a common primary bone tumor in children and adolescents. Circular RNA (circRNA)-IARS acts as an oncogene in multiple human tumors. However, the circ-IARS function in OS is unclear. This research aimed to elucidate the roles and mechanisms of circ-IARS in OS. In this study, circ-IARS expressions were raised in OS tissues and cells. circ-IARS expressions were closely related to clinical stage and distant metastasis. Furthermore, overall survival rates were reduced in OS patients with high circ-IARS levels. Also, silencing circ-IARS weakened OS cell proliferation and invasion, yet enhanced cell ferroptosis. Mechanistically, circ-IARS targeted miR-188-5p to regulate RAB14 expressions in OS cells. Moreover, circ-IARS knockdown repressed OS cell proliferation, invasion, and induced ferroptosis, yet these impacts were abolished by co-transfection with anti-miR-188-5p or pcDNA-RAB14. Meanwhile, interference with circ-IARS reduced OS cell proliferation, and decreased RAB14 (a member of the RAS oncogene family), GPX4, and xCT (crucial ferroptosis regulators) expressions *in vivo*. In conclusion, circ-IARS facilitated OS progression via miR-188-5p/RAB14.

Key words: circ-IARS; miR-188-5p; RAB14; OS; ferroptosis

Osteosarcoma (OS) is a primary malignant tumor and a prominent cause of tumor-related death in children and adolescents [1, 2]. OS originates from mesenchymal cells and is characterized by rapid invasive growth and a high recurrence rate [3, 4]. According to incomplete statistics, the overall 5-year survival rate of local OS patients is approximately 70%, and only 20% of patients with recurrent and metastatic tumors [5]. In recent decades, chemotherapy and surgical resection have made progress in OS therapy, but OS prognosis is still poor [6]. Accordingly, it is urgent to reveal molecular mechanisms of OS progression, offering novel strategies for OS therapy.

With the advancement of high-throughput sequencing technology, extensive circRNAs have been found in multiple human diseases, and the vast majority of circRNAs own high tissue-specific expression characteristics [7, 8]. Accumulating evidence promulgates that circRNA functions in tumorigenesis including OS are diverse. For instance, circRBMS3 modulates eIF4B and YRDC by sponging miR-424-5p, and circRBMS3 knockdown represses OS malignant phenotype [9]. circ_0002137 slows down OS progression via modulating miR-433-3p/IGF1R, supplying a potential target for OS remedy [10]. circ-IARS, also known as circ_0006702, is derived from the isoleucyl-tRNA synthetase 1 (IARS) gene and is implicated in functioning in human tumors. In non-small cell lung cancer, circ-IARS mediates the malignant development of non-small cell lung cancer cells through miR-1252-5p/HDGF [11]. In pancreatic cancer, high circ-IARS expressions are positively correlated with liver metastasis, and tumor node metastasis (TNM) stage of pancreatic cancer, and circ-IARS overexpression accelerates pancreatic cancer cell growth via miR-122/ZO-1 [12]. So far, circ-IARS impacts in OS are unclear. In this research, our data tentatively revealed the high circ-IARS expressions in OS, implying that circ-IARS might be an oncogene in OS.

In the current study, we validated high circ-IARS expressions in OS. At the same time, we investigated circ-IARS functions in OS by decreasing its expressions. Our data suggested that interference with circ-IARS restrained OS cell proliferation and invasion, but induced ferroptosis. Based on

these findings, we further elucidated the circ-IARS mechanism in OS, aiming to offer novel ideas for OS clinical remedy.

Patients and methods

Clinical tissues. OS and corresponding paracancer tissues (50 cases) were collected from The People's Hospital of Luzhou. All patients were informed of this study design and provided with written informed consent. This research was approved by the medical ethics committee of The People's Hospital of Luzhou (LZPH-QR-21017).

Cell culture. Four OS cells (U2OS, HOS, Saos2, and MG63) and human osteoblast cell line hFOB were purchased from the Chinese Academy of Sciences Cell Bank (Shanghai, China). U2OS cells were put in RPMI-1640 (G-CLONE, Beijing, China) with 10% FBS (MedChemExpress, Shanghai, China). HOS, Saos2, MG63, and hFOB cells were grown in DMEM (G-CLONE) containing 10% FBS. All cells were cultured at 37 °C, 5% CO_2.

Cell infection, transfection, and treatment. Lentiviral vectors of negative control and sh-circ-IARS#1, sh-circ-IARS#2, and sh-circ-IARS#3 were produced by Sangon (Shanghai, China). Lentivirus carrying the above-mentioned vectors was generated in HEK293T cells. OS cells were infected with lentivirus with multiplicity of infection (MOI) of 30, and stable OS cells infected with sh-circ-IARS#1, sh-circ-IARS#2, sh-circ-IARS#3 were screened with 5 μg/ml purinamycin [13].

miR-188-5p mimic, anti-miR-188-5p, pcDNA-RAB14, and their corresponding controls were obtained from RiboBio (Guangzhou, China). miR-188-5p mimic, anti-miR-188-5p, or pcDNA-RAB14 was transfected into OS cells with Lipofectamine 3000 (G-CLONE). 48 h later, transfected OS cells were harvested to conduct subsequent assays.

To enunciate regulation of Fe^{2+} levels in OS cells by circ-IARS, OS cells transfected with sh-circ-IARS were exposed to 5 μM erastin (ferroptosis activator, MedChemExpress, HY-15763, 99.57%) or 1 μM ferrostatin-1 (ferroptosis inhibitor, MedChemExpress, HY-100579, 99.96%) for 1 day [14].

Quantitative real-time PCR (qRT-PCR). After total RNA was obtained from OS tissues and cells (U2OS, and HOS) with TRIzol (Beyotime, Shanghai, China), RNA contents and purity were examined by a QNano spectrophotometer (Yeasen, Shanghai, China). For circRNA and mRNA, complementary DNA (cDNA) was synthesized by HyperScript™ First-Strand cDNA Synthesis Kits (Apexbio, Shanghai, China). For miRNA, cDNA was gathered using miRNA Reverse Transcription Kits (Hifunbio, Shanghai, China). RT-PCR was conducted using a SYBR Green I (G-CLONE) on an Mx3000P system (Stratagene, Santa Clara, USA). The procedure was listed: 95 °C for 30 s (denaturation), followed by 40 cycles of denaturation at 95 °C for 5 s, 55 °C for 30 s (annealing), and 72 °C for 30 s (extension). GAPDH (for circRNAs and mRNAs) and U6 (for miRNAs) were endogenous controls. The relative level was determined with $2^{-\Delta\Delta Ct}$. Primer sequences are listed in Table 1.

Table 1. Primer sequences.

Gene name	Primer sequence (5'-3')
circ-IARS	Forward: CCAACATTACAGACCGGTG
	Reverse: CTCGAAGTTGGAAAGTGGAGTG
miR-188-5p	Forward: CACGCACATCCCTTGCAT
	Reverse: CCAGTGCAGGGTCCGAGGTA
U6	Forward: CTCAGAATCACCCAATGC
	Reverse: ATGTTCATCCAGTTGTCAC
GAPDH	Forward: AGGGGCCATCCACAGTCTTC
	Reverse: AGAAGGCTGGGGCTCATTTG

Cell Counting Kit-8 (CCK-8) assay. OS cell viability was checked with Cell Counting Kit-8 (CCK-8) Kits (Mlbio, Shanghai, China). OS cells (6,000 cells/well) were put in 96-well plates and the culture medium was replaced by a medium with 10% CCK-8. OS cells were further cultured for another 1.5 h. Optical density was tested with a microplate reader (Molecular Devices, Shanghai, China) at 450 nm.

Transwell analysis. OS cell invasion was examined by Transwell chambers (8 μm pore size, Corning, USA). OS cells (5×10^4) were grown in upper chambers with serum-free DMEM (200 μl). Simultaneously, DMEM containing 10% FBS was added to lower chambers. After 1 d, OS cells on the surface the below membrane were fixed using 4% paraformaldehyde (Noninbio, Shanghai, China) and dyed with crystal violet (0.1%). Cells on the surface above the membrane were wiped with a cotton swab. Invasive OS cells were assessed under an inverted light microscope (ThermoFisher Scientific, MA, USA) and photographed for preservation.

Detection of Fe^{2+} levels and reactive oxygen species (ROS) levels. Fe^{2+} and ROS levels in OS cells were determined as previously reported methods [15, 16]. Fe^{2+} levels were quantified via Iron Assay Kits (Sigma-Aldrich, Shanghai, China). ROS levels were examined by Reactive Oxygen Species Assay Kits (Yeasen) with the fluorescence microscope (ThermoFisher Scientific).

Western blot. Total proteins were collected with RIPA buffer (Beyotime Biotechnology, Nantong, China). Followed by protein contents were determined via BCA Protein Assay Kits (Mlbio), proteins (15 μg) were separated on 10% SDS-PAGE (Mlbio). Proteins were transferred onto PVDF membranes (Sangon, Shanghai, China). Next, membranes were blocked with 5% non-fat milk, and were further exposed to primary antibodies against GPX4 (ab125066, 1:1000, Abcam, Cambridge, UK), xCT (ab307601, 1:1000, Abcam), RAB14 (K009409M, 1:500, Solarbio, Beijing, China), and GAPDH (ab8245, 1:500, Abcam) overnight at 4 °C, followed by exposing to secondary antibodies Goat Anti-Mouse IgG H&L (HRP) (ab205719, 1:2000, Abcam) or Goat Anti-Rabbit IgG H&L (HRP) (ab205718, 1:2000, Abcam). Signals were visualized using Enhanced Chemiluminescence Kits (Yeasen).

Database analysis. Online websites "starBase" (http://starbase.sysu.edu.cn/), "circBank" (www.circbank.cn) and "circatlas" (https://ngdc.cncb.ac.cn/circatlas/) were applied to forecast miRNAs targeted by circ-IARS, and three were found at intersection: hsa-miR-188-5p, hsa-miR-873-3p, and hsa-miR-4761-3p.

RNA pull-down. Binding of circ-IARS to miR-188-5p, miR-873-3p, or miR-4771-3p was verified using RNA pull-down. To generate probe-coated beads, the circ-IARS probe and control probe were exposed to Dynabeads M-280 Streptavidin beads (ThermoFisher Scientific) for 2.5 h. Soon afterward, OS cell lysates were incubated with circ-IARS or a control probe overnight. RNA complexes bound to microspheres were extracted, and RNA levels were further tested with qRT-PCR.

Dual-luciferase reporter gene assay. The relationship between circ-IARS and miR-188-5p/RAB14 was validated via the dual-luciferase reporter gene assay. A 3'-UTR fragment or mutant fragment containing miR-188-5pp binding sites in circ-IARS and RAB14 mRNA was cloned into the PGL3 luciferase reporter vector (Youbio, Hunan, China). Wild-type (WT) or mutant-type (MUT) luciferase reporter vectors containing circ-IARS-WT, circ-IARS-MUT, RAB14 3'-UTR-WT, and RAB14 3'-UTR-MUT were constructed, respectively. Next, miR-188-5p mimic combined with the above luciferase reporter vectors were cotransfected into OS cells with Lipofectamine 2000 (Solarbio). After 3 d, luciferase activity was determined with a Luciferase Reporter Assay System (ThermoFisher Scientific).

RNA immunoprecipitation (RIP)-qRT-PCR. circ-IARS and miR-188-5p expressions in immunoprecipitation complexes were measured using Magna RNA-binding Protein Immunoprecipitation Kits (Sigma-Aldrich). OS cells were harvested and lysed with RIP lysis. Next, magnetic beads coated with anti-Ago2 (ab186733, 1:40, Abcam) or anti-IgG (ab133470, 1:1000, Abcam) were exposed to cell lysate at 4 °C. circ-IARS and miR-188-5p expressions were tested via qRT-PCR.

***In vivo* study.** Ten BALB/C nude mice (5 weeks of age,18–25 g) were bought from Biocytogen (Beijing, China). Mice were raised in a 12/12 h light/dark cycle at 18–22 °C and 50–60% humidity. All animal experiments were reviewed and approved by the ethics committee of The People's Hospital of Luzhou (LZPH-QR-21017).

After one week of adaptive feeding, HOS cells (2×10^6, 100 µl) transfected with sh-NC and sh-circ-IARS were injected subcutaneously into nude mice (n=5) [17]. Tumor volume was tested weekly, and the calculation formula was: Volume = (long diameter × short diameter)^2 × 0.5 [18]. After 5 weeks, mice were killed with cervical dislocation, and mice were anesthetized with 100 mg/kg pentobarbital sodium to relieve pain during euthanasia [19]. Mouse tumor tissues were preserved in 4% paraformaldehyde (Solarbio).

Immunohistochemistry assay. OS tissues were embedded with paraffin and cut into 5 µm slices. Then, slices were exposed to antibodies against Ki-67 (ab15580, 1 µg/ml, Abcam), RAB14 (K009152P, 1:50, Solarbio), GPX4 (ab125066, 1:1000, Abcam) and xCT (ab307601, 1:500, Abcam). Slices were further counterstained with hematoxylin (Solarbio). Images were obtained with a microscope.

Statistical analysis. Experimental data were listed as mean ± SD. A comparison between the two groups was conducted with Student's t-test. Meanwhile, a comparison among multiple groups was assessed using a one-way analysis of variance (ANOVA) followed by Tukey's post hoc test. Overall survival rates of OS patients with low circ-IARS expressions (n=25) and high circ-IARS expressions (n=25) were checked via Kaplan-Meier survival curve analysis. The difference between groups was considered to be statistically significant when $p<0.05$.

Results

circ-IARS is highly expressed in OS. Initially, we attempted to clarify the circ-IARS expression pattern in OS. As emerged in Figure 1A, circ-IARS expressions in OS tissues

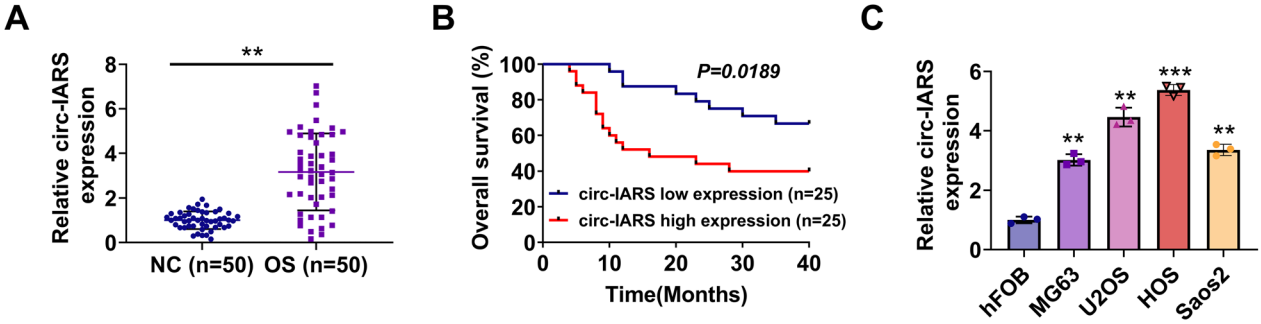

Figure 1. Validation of circ-IARS expressions in osteosarcoma (OS). A) circ-IARS expressions in OS tissues and adjacent tissues were tested using quantitative real-time PCR (qRT-PCR). B) OS patients (n=50) were grouped into low circ-IARS expressions (n=25) and high circ-IARS expressions (n=25). Overall survival rates of OS patients with low circ-IARS expressions (n=25) and high circ-IARS expressions (n=25) were estimated with Kaplan-Meier survival curve analysis. C) circ-IARS expressions in OS cells (U2OS, HOS, Saos2, and MG63) and human osteoblast cell line hFOB were examined with qRT-PCR. **p<0.01 vs. NC, hFOB; ***p<0.001 vs. hFOB. Abbreviations: NC-negative control; OS-osteosarcoma

(n=50) were dramatically higher than those in adjacent tissues (n=50). The median expression value of circ-IARS in OS tissues in Figure 1A was taken as the cut-off value. Patients with OS (n=50) were grouped into low circ-IARS expressions (n=25) and high circ-IARS expressions (n=25). We further proved that circ-IARS expressions were closely interrelated to clinical stage and distant metastasis, but not to patient age, gender, tumor size, and location (Table 2). Meanwhile, overall survival rates were reduced in high circ-IARS expressions (p=0.0189, Figure 1B). Also, circ-IARS expressions were increased in OS cells in contrast to control cells (Figure 1C). Taken altogether, circ-IARS was overexpressed in OS tissues and cells.

Knockdown of circ-IARS represses OS cell proliferation and invasion. To enucleate circ-IARS's impact on OS progression *in vitro*, loss-of-function experiments were conducted in OS cells. Compared with sh-NC, sh-circ-IARS#1, sh-circ-IARS#2, and sh-circ-IARS#3 effectively knocked down circ-IARS in OS cells (Figure 2A). sh-circ-IARS#3 possessed the lowest knock efficiency and was named sh-circ-IARS. The CCK-8 assay further authenticated that interference with circ-IARS weakened OS cell viability (Figure 2B). Additionally, silencing circ-IARS decreased OS cell invasion in contrast to controls (Figure 2C). These data hinted that interference with circ-IARS restrained OS cell proliferation and invasion.

Silencing circ-IARS induces ferroptosis in OS cells. Previous studies validate that ferroptosis modulates OS progression and takes part in OS therapy [20, 21]. Thus, we sought to illuminate whether circ-IARS mediated OS cell ferroptosis. As disclosed in Figures 3A and 3B, circ-IARS knockdown raised Fe^{2+} levels in OS cells, and erastin (ferroptosis activator) further enhanced this raise, while ferrostatin 1 (ferroptosis inhibitor) decreased Fe^{2+} levels in OS cells (Figure 3B). Excessive accumulation of ROS induces ferroptosis in OS cells [22]. Immunofluorescence further expounded that interference with circ-IARS increased ROS levels in OS cells (Figure 3C). Moreover, knocking down circ-IARS lessened GPX4, and xCT (crucial ferroptosis regulators) protein levels (Figure 3D). All the above findings implied that circ-IARS knockdown accelerated OS cell ferroptosis.

Table 2. Correlations of circ-IARS expressions with clinicopathologic features of osteosarcoma.

Characteristic	All cases	circ-IARS expressions		p-value
		High (n=25)	Low (n=25)	
Age (years)				0.556
<20	32	17	15	
≥20	18	8	10	
Gender				0.747
Female	37	19	18	
Male	13	6	7	
Tumor size (cm)				0.355
<5	15	9	6	
≥5	35	16	19	
Distant metastasis				0.047*
Yes	27	17	10	
No	23	8	15	
Clinical stage				0.021*
I+II	30	11	19	
III	20	14	6	
Tumor location				0.306
Tibia/Femur	39	21	18	
Other location	11	4	7	

Note: A chi-square test was used for comparing groups between low and high circ-IARS expressions; *p<0.05

circ-IARS targets miR-188-5p to regulate RAB14 protein levels in OS cells. Subsequently, we further enunciated the prospective mechanism of circ-IARS mediating OS cell growth. We found three miRNAs (hsa-miR-188-5p, hsa-miR-873-3p, and hsa-miR-4761-3p) by taking the intersection of databases predicting circ-IARS targeting miRNAs (Figure 4A). RNA pull-down further revealed that the biotinylated circ-IARS probe enriched more miR-188-5p (Figure 4B). Accordingly, miR-188-5p was selected for follow-up studies. Meanwhile, miR-188-5p mimic effectively overexpressed miR-188-5p in OS cells (Figure 4C). Sites of circ-IARS targeting miR-188-5p and RAB14 targeting miR-188-5p were emerged in Figures 4D and 4E. Furthermore, miR-188-5p mimic reduced luciferase activity in OS cells, and the inhibitory effect disappeared after binding sites of circ-IARS and miR-188-5p or RAB14 3'-UTR and miR-188-5p were mutated (Figures 4F, 4G). Also, anti-Ago2 enriched more circ-IARS and miR-188-5p in contrast to anti-IgG (Figure 4H). To sum up, circ-IARS positively regulated RAB14 expressions via targeting miR-188-5p.

circ-IARS modulates OS cell proliferation, invasion, and ferroptosis through miR-188-5p/RAB14. To ascertain whether circ-IARS mediated OS cell progression via miR-188-5p/RAB14, we knocked down circ-IARS and co-transfected OS cells with anti-miR-188-5p or pcDNA-RAB14. qRT-PCR stated that anti-miR-188-5p effectively knocked down miR-188-5p in OS cells (Figure 5A). Meanwhile, pcDNA-RAB14 transfection overexpressed RAB14 protein levels in OS cells (Figure 5B). On this basis, circ-IARS knockdown reduced OS cell proliferation, while co-transfection with anti-miR-188-5p or pcDNA-RAB14 reversed this reduction (Figure 5C). Transwell analysis of OS cell invasion displayed an analogous trend (Figure 5D). Furthermore, interference with circ-IARS raised Fe^{2+} levels in OS cells, yet this raise was abolished after co-transfection with anti-miR-188-5p or pcDNA-RAB14 (Figure 5E). Also, silencing circ-IARS increased ROS levels in OS cells, while co-transfection of anti-miR-188-5p or pcDNA-RAB14 abolished this increase (Figure 5F). In summary, circ-IARS knockdown weakened OS cell proliferation and invasion, and induced ferroptosis via miR-188-5p/RAB14.

Interference with circ-IARS represses OS cell proliferation *in vivo*. To further elucidate the oncogene function of

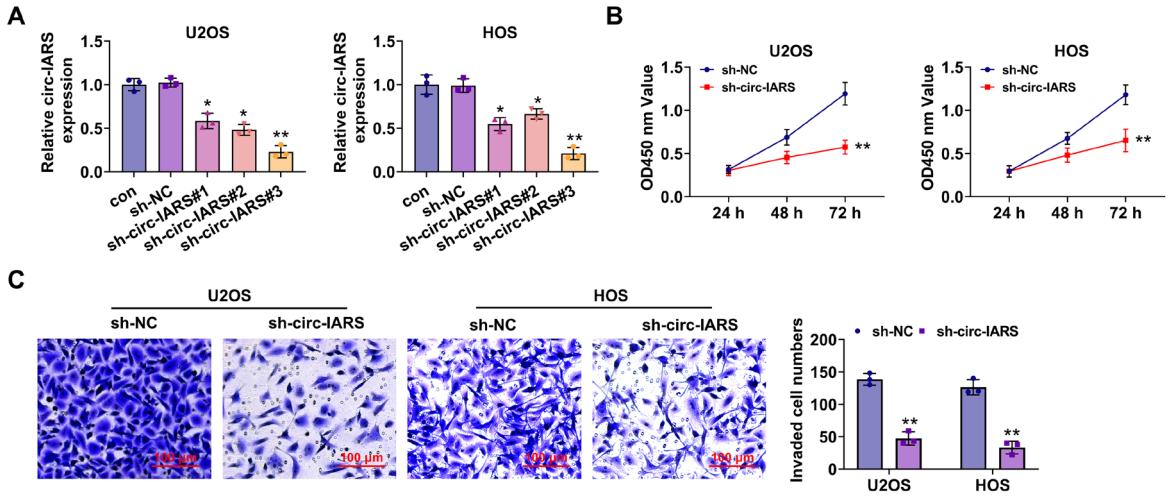

Figure 2. circ-IARS mediates OS cell proliferation and invasion. A) OS cells were infected with sh-circ-IARS#1, sh-circ-IARS#2, and sh-circ-IARS#3 lentivirus for 3 d. qRT-PCR analysis of circ-IARS expressions in OS cells. B) OS cells were infected with sh-circ-IARS#3 (also named sh-circ-IARS) lentivirus for 3 d. OS cell viability was evaluated at different periods (24, 48, and 72 h) via Cell Counting Kit-8 (CCK-8) assay. C) Transwell analysis of OS cell invasion (scale bar: 100 μM). *p<0.05, **p<0.01 vs. control, sh-NC. Abbreviation: Con-control

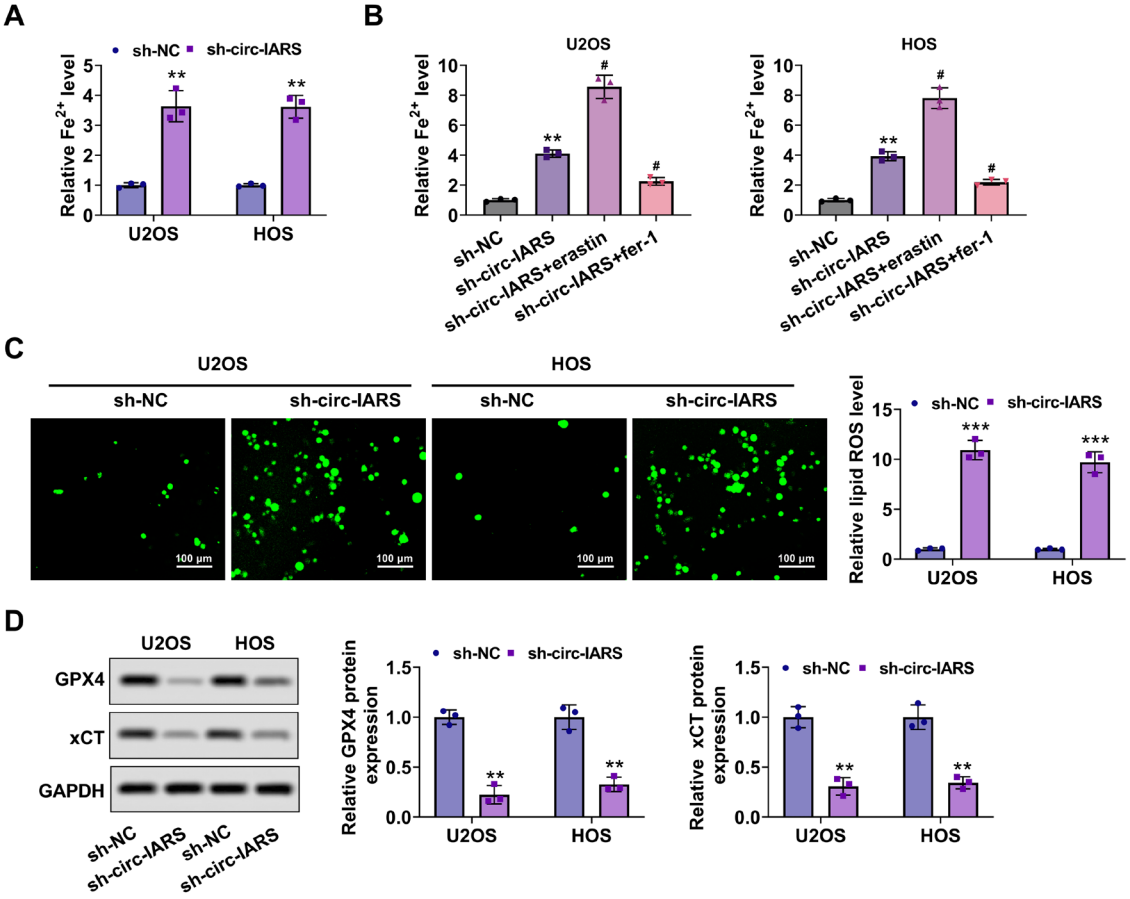

Figure 3. circ-IARS mediates ferroptosis in OS cells. OS cells were infected with sh-circ-IARS lentivirus for 3 d. A) Fe^{2+} levels in OS cells were tested with commercial kits. B) Followed by OS cells were infected with sh-circ-IARS lentivirus for 3 d, OS cells were further exposed to 5 μM erastin (ferroptosis activator) or 1 μM ferrostatin-1 (ferroptosis inhibitor) for 24 h. Fe^{2+} levels in OS cells were examined using commercial kits. C) Immunofluorescence analysis of reactive oxygen species (ROS) levels in OS cells (scale bar: 100 μM). D) Ferroptosis regulators (GPX4 and xCT) protein levels were determined via western blot. **p<0.01, ***p<0.001 vs. sh-NC. #p<0.05 vs. sh-circ-IARS

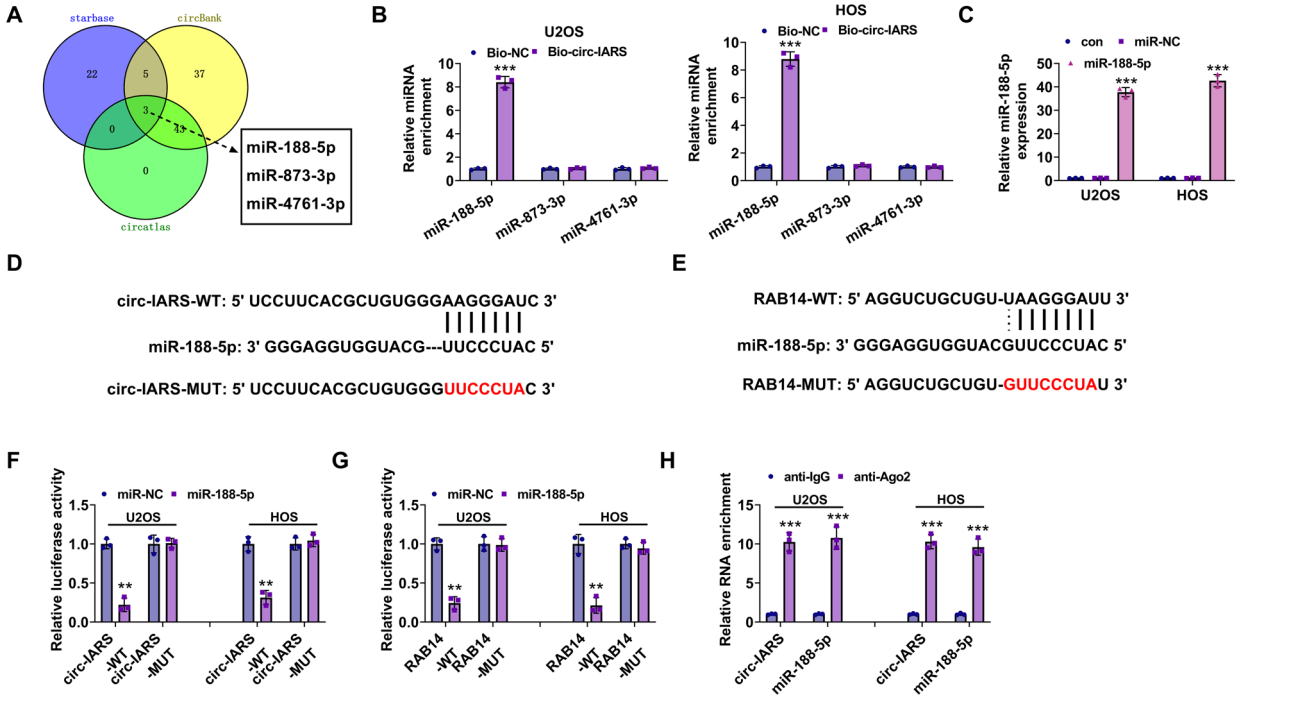

Figure 4. circ-IARS mediates RAB14 expressions through miR-188-5p. A) circ-IARS targeting three miRNAs (hsa-miR-188-5p, hsa-miR-873-3p, and hsa-miR-4761-3p) were found through taking the intersection of three databases ("starBase", "circBank", and "circatlas"). B) RNA pull-down experiments were applied to verify the binding of circ-IARS with hsa-miR-188-5p, hsa-miR-873-3p, or hsa-miR-4771-3p. C) miR-188-5p mimic was transfected into OS cells for 48 h. miR-188-5p expressions were tested with qRT-PCR. D, E) Binding sites of circ-IARS targeting miR-188-5p, and RAB14 targeting miR-188-5p. F, G) Luciferase activity in OS cells was examined via a dual-luciferase reporter gene assay. H) RNA immunoprecipitation (RIP)-qRT-PCR analysis of the relationship of circ-IARS and miR-188-5p. **p<0.01 vs. miR-NC. ***p<0.001 vs. Bio-NC, miR-NC, anti-IgG

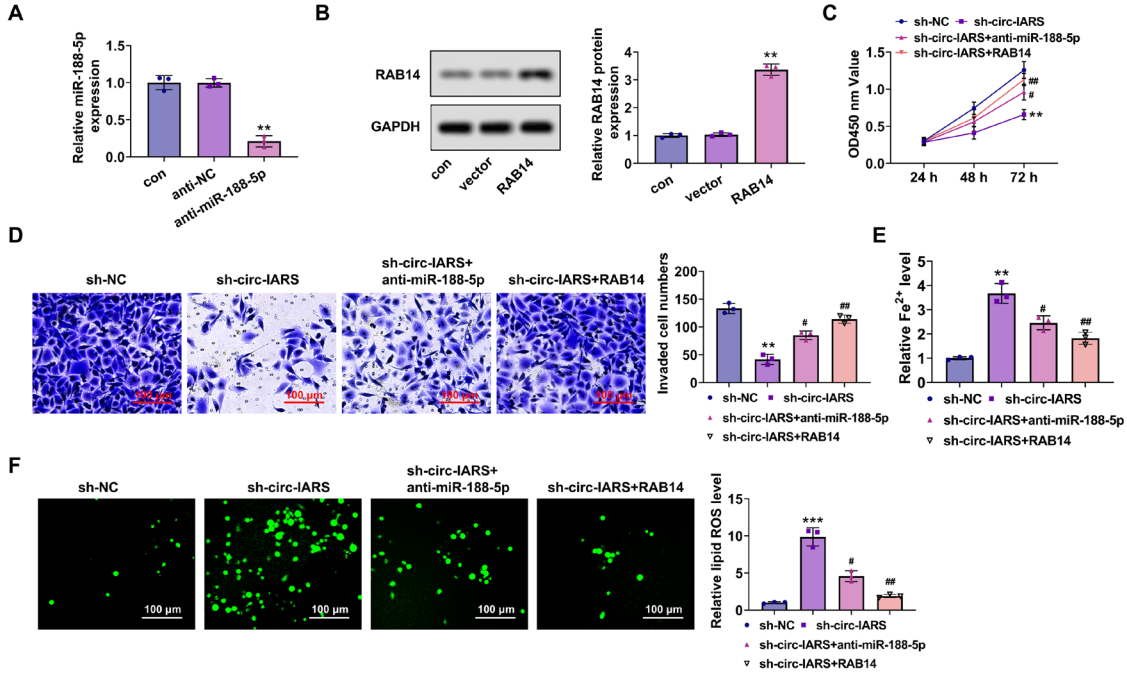

Figure 5. circ-IARS influences OS cell proliferation, invasion, and ferroptosis through miR-188-5p/RAB14. A) anti-miR-188-5p was transfected into OS cells for 48 h. miR-188-5p expressions were examined using qRT-PCR. B) pcDNA-RAB14 was transfected into OS cells for 48 h. Western blot analysis of RAB14 protein levels. C) After circ-IARS was knocked down in OS cells, anti-miR-188-5p or pcDNA-RAB14 was co-transfected into OS cells for 48 h. CCK-8 analysis of OS cell viability at different periods (24, 48, and 72 h). D) OS cell invasion was examined with Transwell assay (scale bar: 100 μM). E) Fe^{2+} levels in OS cells were tested via commercial kits. F) ROS levels in OS cells were tested using an immunofluorescence assay (scale bar: 100 μM). **p<0.01 vs. anti-NC, vector, sh-NC; ***p<0.001 vs. sh-NC; #p<0.05; ##p<0.01 vs. sh-circ-IARS.

circ-IARS in OS, OS cells transfected with sh-circ-IARS were injected subcutaneously into mice. As emerged in Figure 6A, we implied a noticeable reduction in subcutaneous tumor volume in sh-circ-IARS. Analogously, knocking down IARS reduced subcutaneous tumor weight in mice (Figure 6B). Meanwhile, silencing circ-IARS decreased circ-IARS expressions, but increased miR-188-5p expressions (Figure 6C). IHC validated that staining positive rates of Ki-67, RAB14, GPX4, and xCT were reduced after knocking down circ-IARS (Figures 6D, 6E). Collectively, silencing circ-IARS restrained OS cell proliferation *in vivo*.

Discussion

The 5-year survival rate of OS is very low [23], and seriously endangers human health. circRNAs have been identified to exert momentous functions in OS. Nevertheless, circ-IARS roles in OS development remain unreported. Here, we sought to elucidate circ-IARS function in OS and prospective mechanism. Central findings are listed: 1) circ-IARS was highly expressed in OS tissues and cells, and silencing circ-IARS reduced OS cell proliferation and invasion, yet induced ferroptosis. 2) circ-IARS bound to miR-188-5p to mediate RAB14 expressions in OS cells, and circ-IARS knockdown repressed OS cell proliferation and invasion, and boosted ferroptosis via miR-188-5p/RAB14. 3) Interference with circ-IARS reduced OS cell proliferation *in vivo*. Principal findings are shown in Figure 7. This research offered a novel regulatory axis for OS development: circ-IARS/miR-188-5p/RAB14.

Accumulating studies authenticate that circ-IARS takes part in mediating the prognosis of multiple tumors. Such as circ-IARS expressions are positively correlated with TNM stage in pancreatic cancer, and negatively correlated with postoperative survival [12]. circ-IARS expressions are raised in serum exosomes of patients with non-small cell lung cancer, hinting that circ-IARS is a novel potentially carcinogenic molecule in non-small cell lung cancer [11]. As

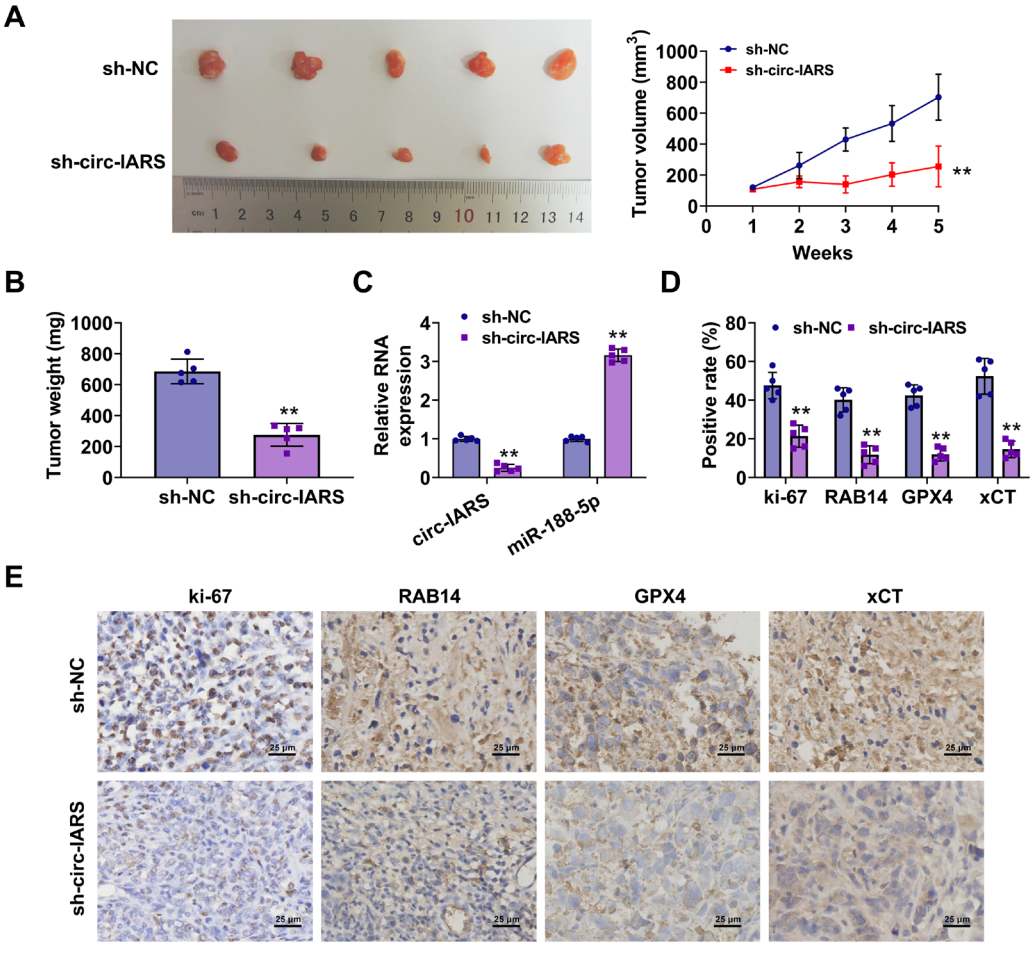

Figure 6. circ-IARS regulates OS cell proliferation *in vivo*. OS cells transfected with sh-circ-IARS (2×10^6) were injected subcutaneously into mice. A) Detection of tumor volume. (B) Analysis of tumor weight. (C) circ-IARS and miR-188-5p expressions were examined using qRT-PCR. (D–E) Ki-67, RAB14, GPX4, and xCT expressions were identified by immunohistochemistry assay (scale bar: 25 μM). **p<0.01 vs. sh-NC

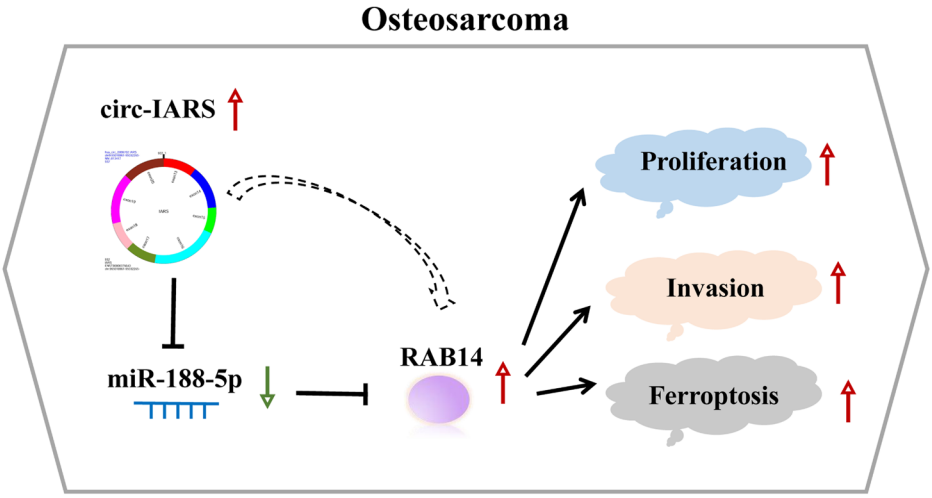

Figure 7. circ-IARS modulates OS cell proliferation, invasion, and ferroptosis through miR-188-5p/RAB14.

expected, our research illustrated that circ-IARS expressions were closely related to clinical stage and distant metastasis, which implied that circ-IARS was a potential prognostic marker for OS.

It is well known that abnormal cancer cell proliferation and invasion accelerate OS progression. For instance, knocking down circ_0001174 alleviates the OS process by restraining OS cell proliferation and invasion [24]. Downregulation of circSRSF4 reduces OS cell proliferation and invasion via miR-224/Rac1 [25]. The above research data vindicated that targeting to repress OS cell proliferation and invasion is expected to mitigate OS. Correspondingly, our research also proved that silencing circ-IARS reduced OS cell proliferation and invasion.

Ferroptosis is a novel form of programmed cell death discovered in recent years [26]. As has been reported, ferroptosis is bound up with iron overload as well as ROS accumulation [27]. Critically, accumulated evidence elucidates that ferroptosis takes part in mediating the OS process. For example, curcumin induces OS cell ferroptosis through Nrf2/GPX4, hinting that curcumin has a therapeutic effect on the OS model [28]. Stearoyl-CoA desaturase induces OS ferroptosis *in vitro* and *in vivo*, implying that Stearoyl-CoA desaturase is a potential target for OS remedy [29]. Notably, circ-IARS acts as an oncogene in non-small-cell lung cancer, and circ-IARS knockdown promotes apoptosis of non-small-cell lung cancer cells [11]. As expected, we further elucidated that silencing circ-IARS raised Fe^{2+} levels and ROS levels in OS cells, suggesting that silencing circ-IARS enhanced OS cell ferroptosis. On this basis, we next probed into the circ-IARS mechanism in OS.

circRNAs function through a variety of mechanisms, such as acting as microRNA (miRNA) sponges to reduce their regulatory effect on mRNAs [30]. Accumulating evidence substantiates the critical roles of miRNAs in numerous human diseases and miRNAs take part in cellular biological processes containing cell proliferation and apoptosis [31, 32]. Recently, the regulatory function of miRNAs in OS has been gradually confirmed. For example, miR-708 is lessened in OS cell lines and mediates OS cell growth via targeting CUL4B [33]. miR-221 represses the Wnt axis and enhances OS cell proliferation through targeting FBXW11 [34]. In the current research, we identified three miRNAs targeting circ-IARS via database: hsa-miR-188-5p, hsa-miR-873-3p, and hsa-miR-4761-3p. Meanwhile, biotinylated circ-IARS probes enriched more miR-188-5p. miR-188-5p has been repeatedly reported to mediate the progression of malignant tumors, mainly consisting of gastric cancer [35], ovarian cancer [36], and breast cancer [37]. Crucially, the upregulation of miR-188-5p weakens OS cell activity, implying that miR-188-5p is a potential target for OS therapy [38]. Meanwhile, miR-188-5p is regulated by multiple lncRNAs during the progression of malignant tumors, containing LINC00491 [39], and lncRNA SNHG15 [40]. Similarly, we also demonstrated that circ-IARS targeted miR-188-5p in OS cells.

Next, we further illustrated downstream targets of miR-188-5p. Our research expounded that miR-188-5p binding sites existed in RAB14 3'-UTR, and miR-188-5p mimic reduced luciferase activity in RAB14-WT cells. RAB14 is a notable member of the RAS oncogene family [41]. RAB14 is an oncogene in multiple cancer types containing OS. For instance, silencing RAB14 represses OS development, and miR-451 is an upstream target of RAB14 [42]. RAB14 is a downstream target of miR-338-3p, and CASC15 accelerates OS cell growth through upregulating RAB14, hinting that CASC15/miR-338-3p/RAB14 is a possible therapeutic axis for OS patients [43]. Similar to these findings, our experimental data also suggested that miR-188-5p targeted RAB14, and circ-IARS mediated RAB14 protein levels in OS cells through miR-188-5p. Also, silencing circ-IARS weakened

OS cell proliferation and invasion, while inducing ferroptosis via miR-188-5p/RAB14. Notably, circ-IARS knockdown reduced OS cell proliferation *in vivo*. There are some limitations in our study as 1) possible signaling axes were not to be studied, 2) gain-of-function for circ-IARS assays were not explored, and 3) the phenotypes in this study lacked oxidative stress, immune response, etc.

In summary, we found that circ-IARS was an oncogene in OS and participated in OS development via miR-188-5p/RAB14. Our experimental data hinted that circ-IARS/miR-188-5p/RAB14 might be a novel regulatory mechanism for OS.

References

[1] NOONE AM, CRONIN KA, ALTEKRUSE SF, HOWLADER N, LEWIS DR et al. Cancer Incidence and Survival Trends by Subtype Using Data from the Surveillance Epidemiology and End Results Program, 1992–2013. Cancer Epidemiol Biomarkers Prev 2017; 26: 632–641. https://doi.org/10.1158/1055-9965.Epi-16-0520

[2] LI S, ZHANG H, LIU J, SHANG G. Targeted therapy for osteosarcoma: a review. J Cancer Res Clin Oncol 2023; 149: 6785–6797. https://doi.org/10.1007/s00432-023-04614-4

[3] YE G, JIAO Y, DENG L, CHENG M, WANG S et al. Beauvericin suppresses the proliferation and pulmonary metastasis of osteosarcoma by selectively inhibiting TGFBR2 pathway. Int J Biol Sci 2023; 19: 4376–4392. https://doi.org/10.7150/ijbs.86214

[4] ZHANG J, LI N, LU S, CHEN Y, SHAN L et al. The role of Notch ligand Jagged1 in osteosarcoma proliferation, metastasis, and recurrence. J Orthop Surg Res 2021; 16: 226. https://doi.org/10.1186/s13018-021-02372-y

[5] PANEZ-TORO I, MUÑOZ-GARCÍA J, VARGAS-FRANCO JW, RENODON-CORNIÈRE A, HEYMANN MF et al. Advances in Osteosarcoma. Curr Osteoporos Rep 2023; 21: 330–343. https://doi.org/10.1007/s11914-023-00803-9

[6] JAFARI F, JAVDANSIRAT S, SANAIE S, NASERI A, SHAMEKH A et al. Osteosarcoma: A comprehensive review of management and treatment strategies. Ann Diagn Pathol 2020; 49: 151654. https://doi.org/10.1016/j.anndiagpath.2020.151654

[7] BACH DH, LEE SK, SOOD AK. Circular RNAs in Cancer. Mol Ther Nucleic Acids 2019; 16: 118–129. https://doi.org/10.1016/j.omtn.2019.02.005

[8] HAN B, CHAO J, YAO H. Circular RNA and its mechanisms in disease: From the bench to the clinic. Pharmacol Ther 2018; 187: 31–44. https://doi.org/10.1016/j.pharmthera.2018.01.010

[9] GONG Z, SHEN P, WANG H, ZHU J, LIANG K et al. A novel circular RNA circRBMS3 regulates proliferation and metastasis of osteosarcoma by targeting miR-424-eIF4B/YRDC axis. Aging (Albany NY) 2023; 15: 1564–1590. https://doi.org/10.18632/aging.204567

[10] ZHANG M, YU GY, LIU G, LIU WD. Circular RNA circ_0002137 regulated the progression of osteosarcoma through regulating miR-433-3p/ IGF1R axis. J Cell Mol Med 2022; 26: 1806–1816. https://doi.org/10.1111/jcmm.16166

[11] YANG J, YANG C, LI P. circ-IARS depletion inhibits the progression of non-small-cell lung cancer by circ-IARS/miR-1252-5p/HDGF ceRNA pathway. Open Med (Wars) 2023; 18: 20220613. https://doi.org/10.1515/med-2022-0613

[12] LI J, LI Z, JIANG P, PENG M, ZHANG X et al. Circular RNA IARS (circ-IARS) secreted by pancreatic cancer cells and located within exosomes regulates endothelial monolayer permeability to promote tumor metastasis. J Exp Clin Cancer Res 2018; 37: 177. https://doi.org/10.1186/s13046-018-0822-3

[13] FU B, LIU W, ZHU C, LI P, WANG L et al. Circular RNA circBCBM1 promotes breast cancer brain metastasis by modulating miR-125a/BRD4 axis. Int J Biol Sci 2021; 17: 3104–3117. https://doi.org/10.7150/ijbs.58916

[14] LI Z, LUO Y, WANG C, HAN D, SUN W. Circular RNA circBLNK promotes osteosarcoma progression and inhibits ferroptosis in osteosarcoma cells by sponging miR-188-3p and regulating GPX4 expression. Oncol Rep 2023; 50: 192. https://doi.org/10.3892/or.2023.8629

[15] DU J, WANG T, LI Y, ZHOU Y, WANG X et al. DHA inhibits proliferation and induces ferroptosis of leukemia cells through autophagy dependent degradation of ferritin. Free Radic Biol Med 2019; 131: 356–369. https://doi.org/10.1016/j.freeradbiomed.2018.12.011

[16] ZHANG H, GE Z, WANG Z, GAO Y, WANG Y et al. Circular RNA RHOT1 promotes progression and inhibits ferroptosis via mir-106a-5p/STAT3 axis in breast cancer. Aging (Albany NY) 2021; 13: 8115–8126. https://doi.org/10.18632/aging.202608

[17] XUE Y, GUO Y, LIU N, MENG X. MicroRNA-22-3p targeted regulating transcription factor 7-like 2 (TCF7L2) constrains the Wnt/β-catenin pathway and malignant behavior in osteosarcoma. Bioengineered 2022; 13: 9135–9147. https://doi.org/10.1080/21655979.2021.2003942

[18] ZHOU B, GE Y, SHAO Q, YANG L, CHEN X et al. Long noncoding RNA LINC00284 facilitates cell proliferation in papillary thyroid cancer via impairing miR-3127-5p targeted E2F7 suppression. Cell Death Discov 2021; 7: 156. https://doi.org/10.1038/s41420-021-00551-8

[19] LIM XR, DRUMM BT, SERGEANT GP, HOLLYWOOD MA, THORNBURY KD. Ca^{2+} -activated Cl^- channels (TMEM16A) underlie spontaneous electrical activity in isolated mouse corpus cavernosum smooth muscle cells. Physiol Rep 2022; 10: e15504. https://doi.org/10.14814/phy2.15504

[20] ZHAO J, ZHAO Y, MA X, ZHANG B, FENG H. Targeting ferroptosis in osteosarcoma. J Bone Oncol 2021; 30: 100380. https://doi.org/10.1016/j.jbo.2021.100380

[21] LIU X, DU S, WANG S, YE K. Ferroptosis in osteosarcoma: A promising future. Fron Oncol 2022; 12: 1031779. https://doi.org/10.3389/fonc.2022.1031779

[22] CHEN W, LI Z, YU N, ZHANG L, LI H et al. Bone-targeting exosome nanoparticles activate Keap1 / Nrf2 / GPX4 signaling pathway to induce ferroptosis in osteosarcoma cells. J Nanobiotechnology 2023; 21: 355. https://doi.org/10.1186/s12951-023-02129-1

[23[HARRIS MA, HAWKINS CJ. Recent and Ongoing Research into Metastatic Osteosarcoma Treatments. Int J Mol Sci 2022; 23: 3817. https://doi.org/10.3390/ijms23073817

[24] LIN F, WANG X, ZHAO X, REN M, WANG Q et al. Circ_0001174 facilitates osteosarcoma cell proliferation, migration, and invasion by targeting the miR-186-5p/MACC1 axis. J Orthop Surg Res 2022; 17: 159. https://doi.org/10.1186/s13018-022-03059-8
[25] SUN X, ZHAO X, XU S, ZHOU Y, JIA Z et al. CircSRSF4 Enhances Proliferation, Invasion, and Migration to Promote the Progression of Osteosarcoma via Rac1. Int J Mol Sci 2022; 23: 6200. https://doi.org/10.3390/ijms23116200
[26] DIXON SJ, LEMBERG KM, LAMPRECHT MR, SKOUTA R, ZAITSEV EM et al. Ferroptosis: an iron-dependent form of nonapoptotic cell death. Cell 2012; 149: 1060–1072. https://doi.org/10.1016/j.cell.2012.03.042
[27] WAN J, REN H, WANG J. Iron toxicity, lipid peroxidation and ferroptosis after intracerebral haemorrhage. Stroke Vasc Neurol 2019; 4: 93–95. https://doi.org/10.1136/svn-2018-000205
[28] YUAN C, FAN R, ZHU K, WANG Y, XIE W et al. Curcumin induces ferroptosis and apoptosis in osteosarcoma cells by regulating Nrf2/GPX4 signaling pathway. Exp Biol Med (Maywood, NJ) 2023; 248: 2183–2197. https://doi.org/10.1177/15353702231220670
[29] NIE J, HE C, SHU Z, LIU N, ZHONG Y et al. Identification and experimental validation of Stearoyl-CoA desaturase is a new drug therapeutic target for osteosarcoma. Eur J Pharmacol 2024; 963: 176249. https://doi.org/10.1016/j.ejphar.2023.176249
[30] PARASKEVOPOULOU MD, HATZIGEORGIOU AG. Analyzing MiRNA-LncRNA Interactions. Methods Mol Biol 2016; 1402: 271–286. https://doi.org/10.1007/978-1-4939-3378-5_21
[31] DIENER C, KELLER A, MEESE E. Emerging concepts of miRNA therapeutics: from cells to clinic. Trends Genet 2022; 38: 613–626. https://doi.org/10.1016/j.tig.2022.02.006
[32] LU M, LU F, LIAO C, GUO Y, MAO C et al. High throughput miRNA sequencing and bioinformatics analysis identify the mesenchymal cell proliferation and apoptosis related miRNAs during fetal mice palate development. J Gen Med 2023; 25: e3531. https://doi.org/10.1002/jgm.3531
[33] CHEN G, ZHOU H. MiRNA-708/CUL4B axis contributes into cell proliferation and apoptosis of osteosarcoma. Eur Rev Med Pharmacol Sci 2018; 22: 5452–5459. https://doi.org/10.26355/eurrev_201809_15805
[34] ZHANG Q, YIN X, ZHANG Y. MicroRNA-221 Promotes Cell Proliferation and Inhibits Apoptosis in Osteosarcoma Cells by Directly Targeting FBXW11 and Regulating Wnt Signaling. Arch Med Res 2021; 52: 191–199. https://doi.org/10.1016/j.arcmed.2020.10.017
[35] PENG Y, SHEN X, JIANG H, CHEN Z, WU J et al. miR-188-5p Suppresses Gastric Cancer Cell Proliferation and Invasion via Targeting ZFP91. Oncol Res 2018; 27: 65–71. https://doi.org/10.3727/096504018x15191223015016
[36] ZHANG H, YUAN N, CHE H, CHEN X. MiR-188-5p inhibits cell proliferation and migration in ovarian cancer via competing for CCND2 with ELAVL1. Cell Mol Biol (Noisy-le-grand) 2023; 69: 69–74. https://doi.org/10.14715/cmb/2023.69.3.9
[37] WANG M, ZHANG H, YANG F, QIU R, ZHAO X et al. miR-188-5p suppresses cellular proliferation and migration via IL6ST: A potential noninvasive diagnostic biomarker for breast cancer. J cell Physiol 2020; 235: 4890–4901. https://doi.org/10.1002/jcp.29367
[38] ZHAO Z, CHEN J, XIA D. Knockdown of HCG18 Inhibits Cell Viability, Migration and Invasion in Pediatric Osteosarcoma by Targeting miR-188-5p/FOXC1 Axis. Mol Biotechnol 2021; 63: 807–817. https://doi.org/10.1007/s12033-021-00343-6
[39] FANG Z, RUAN B, ZHONG M, XIONG J, JIANG Y et al. Silencing LINC00491 Inhibits Pancreatic Cancer Progression through MiR-188-5p-induced Inhibition of ZFP91. J Cancer 2022; 13: 1808–1819. https://doi.org/10.7150/jca.65071
[40] WANG T, LIANG D, YANG H. SNHG15 facilitated malignant behaviors of oral squamous cell carcinoma through targeting miR-188-5p/DAAM1. J Oral Pathol Med 2021; 50: 681–691. https://doi.org/10.1111/jop.13169
[41] LI Y, ZONG M, GUAN X, WU X, MA G et al. MBNL1-AS1 Promotes Hypoxia-Induced Myocardial Infarction via the miR-132-3p/RAB14/CAMTA1 Axis. Oxid Med Cell Longev 2023; 2023: 3308725. https://doi.org/10.1155/2023/3308725
[42] ZHAI Y, LIU M, ZHENG Y. MicroRNA-451 dictates the anoikis resistance of osteosarcoma by targeting Rab14. Int J Clin Exp Pathol 2017; 10: 10989–10997.
[43] ZHANG H, WANG J, REN T, HUANG Y, YU Y et al. LncRNA CASC15 is Upregulated in Osteosarcoma Plasma Exosomes and CASC15 Knockdown Inhibits Osteosarcoma Progression by Regulating miR-338-3p/RAB14 Axis. Onco Targets Ther 2020; 13: 12055–12066. https://doi.org/10.2147/ott.S282053